Available online at www.sciencedirect.com
ScienceDirect
Journal of Non-Crystalline Solids 354 (2008) 224–232
JOURNAL OF NON-CRYSTALLINE SOLIDS
www.elsevier.com/locate/jnoncrysol

Diffusion and reactions of interstitial oxygen species in amorphous SiO_2: A review

Koichi Kajihara [a,b,*], Taisuke Miura [c], Hayato Kamioka [d], Akira Aiba [e], Motoko Uramoto [e], Yukihiro Morimoto [e], Masahiro Hirano [a], Linards Skuja [a,f], Hideo Hosono [a,g]

[a] *Transparent Electro-Active Materials Project, Japan Science and Technology Agency, Frontier Collaborative Research Center, Mail Box S2-13, Tokyo Institute of Technology, 4259 Nagatsuta, Midori-ku, Yokohama 226-8503, Japan*
[b] *Department of Applied Chemistry, Graduate School of Urban Environmental Sciences, Tokyo Metropolitan University, 1-1 Minami-Osawa, Hachioji 192-0397, Japan*
[c] *Laserfront Technologies, Inc., 1120 Shimokuzawa, Sagamihara 229-1198, Japan*
[d] *Graduate School of Pure and Applied Sciences, University of Tsukuba, 1-1-1 Tennodai, Tsukuba 305-8571, Japan*
[e] *Research and Development Center, Ushio Inc., 1194 Sazuchi, Bessho-cho, Himeji 671-0224, Japan*
[f] *Institute of Solid State Physics, University of Latvia, Kengaraga iela 8, LV1063 Riga, Latvia*
[g] *Materials and Structures Laboratory & Frontier Collaborative Research Center, Tokyo Institute of Technology, 4259 Nagatsuta, Midori-ku, Yokohama 226-8503, Japan*

Available online 25 October 2007

Abstract

This article briefly summarizes the diffusion and reactions of interstitial oxygen species in amorphous SiO_2 (a-SiO_2). The most common form of interstitial oxygen species is oxygen molecule (O_2), which is sensitively detectable via its characteristic infrared photoluminescence (PL) at 1272 nm. The PL observation of interstitial O_2 provides key data to verify various processes related to interstitial oxygen species: the dominant role of interstitial O_2 in long-range oxygen transport in a-SiO_2; formation of the Frenkel defect pair (Si–Si bond and interstitial oxygen atom, O^0) by dense electronic excitation; efficient photolysis of interstitial O_2 into O^0 with F_2 laser light ($\lambda = 157$ nm, $h\nu = 7.9$ eV); and creation of interstitial ozone molecule via reaction of interstitial O_2 with photogenerated O^0. The efficient formation of interstitial O^0 by F_2 laser photolysis makes it possible to investigate the mobility, optical absorption, and chemical reactions of interstitial O^0. The observed properties of O^0 are consistent with the model that O^0 takes the configuration of Si–O–O–Si bond. Interstitial O_2 and O^0 react with dangling bonds, oxygen vacancies, and chloride groups in a-SiO_2. Reactions of interstitial O_2 and O^0 with mobile interstitial hydrogen species produce interstitial water molecules and hydroperoxy radicals. Interstitial hydroxyl radicals are formed by F_2 laser photolysis of interstitial water molecules.

PACS: 61.72.Ji; 78.55.Qr; 66.30.Hs; 33.50.Dq

Keywords: Diffusion and transport; Silica

1. Introduction

Amorphous silica (a-SiO_2 or SiO_2 glass) is an important material in modern optics and electronics technologies. Since oxygen is a component of a-SiO_2, diffusion and reactions of oxygen species are closely related to intrinsic phenomena in a-SiO_2. For example, oxygen diffusion in

* Corresponding author. Address: Department of Applied Chemistry, Graduate School of Urban Environmental Sciences, Tokyo Metropolitan University, 1-1 Minami-Osawa, Hachioji 192-0397, Japan.
E-mail address: kkaji@tmu.ac.jp (K. Kajihara).

0022-3093/$ - see front matter © 2007 Elsevier B.V. All rights reserved.
doi:10.1016/j.jnoncrysol.2007.07.038

a-SiO_2 is utilized to fabricate gate dielectric a-SiO_2 films on silicon-based integrated circuits [1]. Radiation-induced displacement and migration of oxygen species in a-SiO_2 create point defects, which degrade the optical and electrical properties of a-SiO_2 [2,3].

The structure of a-SiO_2 is visualized as a continuous network of Si–O bonds, consisting of corner-shared SiO_4 tetrahedra. Each oxygen atom in the network bridges two silicon atoms and is termed 'bridging oxygen' or 'network oxygen'. A distinct structural feature of the network is the presence of network interstices (voids) that enable dissolution and diffusion of small chemical species [4,5].

Oxygen species embedded in the interstitial voids are distinguished from the network oxygen; they migrate through the voids and participate in various chemical and photochemical reactions in a-SiO_2. The purpose of this paper is to present a brief overview of the current understanding of the diffusion and reactions of oxygen species dissolved in the interstitial voids in a-SiO_2. Other excellent articles covering the scope of this paper include Refs. [4–6]. In this article, we describe the properties of interstitial oxygen species including oxygen molecules (O_2), oxygen atoms (O^0), ozone molecules (O_3), and oxygen radicals. Emphasis is placed on the properties of interstitial O_2 because it is the main form of excess oxygen in a-SiO_2. We present the utility of detecting interstitial O_2 via the characteristic infrared photoluminescence to study processes involving the interstitial oxygen species.

2. Interstitial oxygen molecules

2.1. Observation by optical spectroscopy

Raman spectroscopy is a conventional technique to detect diatomic molecules. The presence of interstitial O_2 has been first confirmed by a Raman observation of the O–O stretching mode appeared in a-SiO_2 optical fibers of low hydroxyl (SiOH) concentrations [7], which were prepared by oxidation of $SiCl_4$ in hydrogen-free plasma flame (often termed 'type IV' silica) [8].

Other optical methods to detect interstitial O_2 make use of the electronic transitions in O_2. The ground state O_2 ($X^3\Sigma_g^-$) is triplet wherein the doubly degenerate antibonding π_g orbitals are occupied by two electrons with the same spin. The first and second excited states ($a^1\Delta_g$ and $b^1\Sigma_g^+$) are singlet. As shown in Fig. 1, these states are obtained by just altering the spin and distribution of the two electrons in the two π_g orbitals [9]. Since the a–X and b–X transitions are both spin- and parity-forbidden, optical absorption bands associated with these transitions are very weak. However, the transition probabilities are enhanced by interactions between interstitial O_2 and surrounding Si–O network, which partially relax the parity selection rule. Indeed, the a–X and b–X absorption bands of interstitial O_2 are detectable in O_2-rich optical fibers with a large optical path length [10], and the evaluated absorption cross sections are two orders of magnitude larger than those of O_2 in air [11].

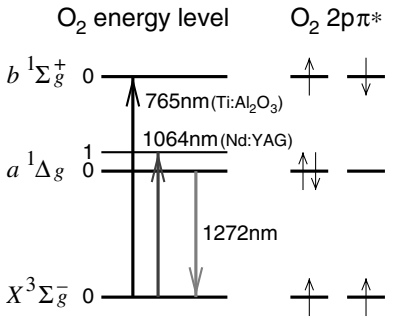

Fig. 1. Schematic diagram of low-lying electronic states and electronic transitions of interstitial O_2 in a-SiO_2.

The a → X transition of interstitial O_2 gives rise to an infrared (IR) photoluminescence (PL) band at ~1272 nm [12]. The same PL band has been recorded by an *in situ* PL observation of a fluorine-doped fiber exposed to neutrons and γ-rays in a nuclear reactor [13]. The PL quantum yield of interstitial O_2 is considered to be larger than 0.1 [14]. Since the interactions with the surrounding Si–O network increase the transition rate, the measured PL decay constant of interstitial O_2 (~0.8 s [15,16]) is much shorter than that of an isolated O_2 molecule (>60 min [17,9]). Such increase in the radiative transition rate is typical of O_2 molecules dissolved in solids or liquids [9]. The decay constant of interstitial O_2 in a-SiO_2 is further decreased by non-radiative transitions caused by SiOH groups [16].

Measurements of the a → X PL band make it possible to detect interstitial O_2, much more sensitively than by the optical absorption or Raman spectroscopy. The 'a' state is efficiently populated via the b ← X transition located at ~765 nm (Fig. 1). Using a titanium sapphire laser to excite the b ← X transition, interstitial O_2 molecules as few as $\sim 10^{14}$ cm^{-3} have been detected [14]. The PL band is also induced by the fundamental wavelengths of Nd:YAG and Nd:YVO_4 lasers ($\lambda \simeq 1064$ nm) [12], which are commonly used as light sources in Fourier-transform IR Raman spectrometers. The efficiency of the excitation at 1064 nm causing the transition from the X state to the first vibronic sideband of the 'a' state (Fig. 1) is two orders of magnitude lower than that at 765 nm. However, the 1064 nm excitation induces both the PL band and the fundamental Raman bands of a-SiO_2 in the same spectral range as shown in Fig. 2, making it possible to evaluate the absolute concentration of interstitial O_2 from the intensity of the PL band normalized to that of the Raman bands of a-SiO_2. The relation between the normalized PL intensity and the concentration of interstitial O_2 has been calibrated using a type IV O_2-rich a-SiO_2 (Suprasil W), whose O_2 concentration was determined from the ratio of the Raman band intensity of interstitial O_2 to that of O_2 in air [18].

Thermal desorption spectroscopy (TDS), which measures the amount of O_2 released by thermal annealing [19], offers a more straightforward way to relate the normalized PL intensity to the concentration of interstitial

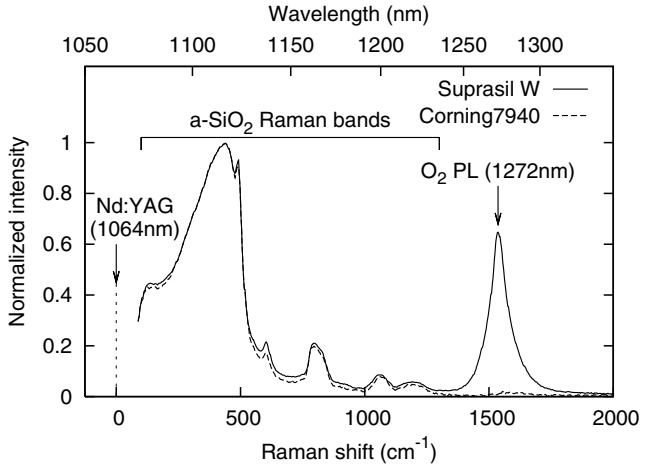

Fig. 2. PL band of interstitial O_2 and fundamental Raman bands of a-SiO_2 induced by excitation with Nd:YAG laser light oscillating at 1064 nm. The 1272 nm PL band is observed in an O_2-rich a-SiO_2 (Suprasil W) whereas does not appear in an O_2-free one (Corning 7940). After Ref. [18].

O_2 [20].[1] Fig. 3(a) shows the result of a recent TDS experiment[2] for an O_2-loaded a-SiO_2 sample (SiF $\sim 1.4\times10^{19}\,cm^{-3}$, SiOH $\sim 1\times10^{18}\,cm^{-3}$; a set of five plates each sized $10\times20\times1$ mm, total volume 1 cm^3, total surface area 23 cm^2), prepared by thermal annealing for 288 h at 1000 °C in an SiOH-free silica tube (inner diameter ~12 mm and wall thickness ~1.2 mm) sealed with ~3 atm O_2 at room temperature. The sample was taken out from the tube just before the TDS measurement, and this procedure greatly suppressed the emission of gases other than O_2 ($m/e = 32$) as compared with the previous report [20]. The number of desorbed O_2 molecules was $\sim 8.3\times10^{16}$ (uncertainty of +20–10%[3]). The main source of H_2O ($m/e = 18$) released above 500 °C is dehydroxylation of the sample. The remaining part of H_2O and other gases may result from adsorbates on the sample.

Fig. 3(b) shows the PL–Raman spectra of the sample before and after the TDS measurement. Since the decrease in the PL intensity corresponds to the concentration change of interstitial O_2, ΔC, of $\sim 7.2\times10^{16}\,cm^{-3}$,[4] the

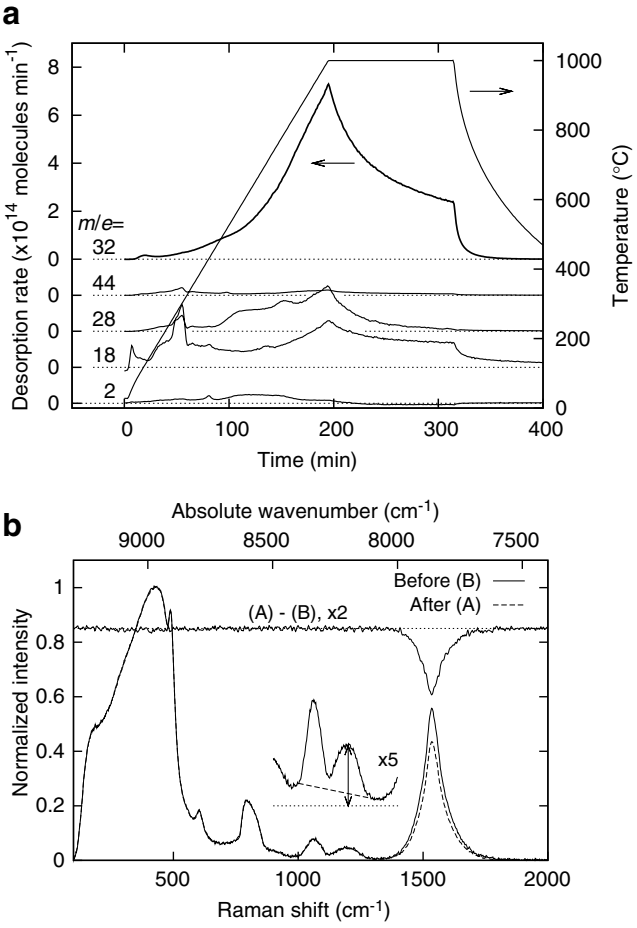

Fig. 3. (a) TDS profiles of O_2 ($m/e = 32$), H_2 (2), H_2O (18), CO + N_2 (28), and CO_2 (44) released from an O_2-loaded a-SiO_2 sample set (SiF $1.4\times10^{19}\,cm^{-3}$, SiOH $\sim 1\times10^{18}\,cm^{-3}$; set of five plates each sized $10\times20\times1$ mm, total volume 1 cm^3). The background gas release from the TDS chamber is subtracted. The numbers of the desorbed molecules were 8.3×10^{16} (O_2), 0.4×10^{16} (H_2), 3.7×10^{16} (H_2O), 1.9×10^{16} (CO + N_2), and 0.3×10^{16} (CO_2). (b) PL–Raman spectra of the O_2-loaded sample measured before and after the TDS experiment. The dashed line in the magnified Raman spectrum of a-SiO_2 shows the baseline used to calculate the integral intensity of the Raman bands, and the two-headed arrow indicates the amplitude at 1200 cm^{-1}.

data shown in Fig. 3(b) yield the relation $\Delta C\ (cm^{-3}) \simeq 4.0\times10^{16}\Delta I_{PL}/I_{Raman}$, where ΔI_{PL} is the change in the integrated intensity of the PL band and I_{Raman} is the intensity of the Raman band of a-SiO_2 arbitrarily defined as an area above a straight line connecting the spectrum points at 1000 and 1300 cm^{-1}. It is also possible to relate ΔC to the ratio of the amplitudes of the PL and Raman bands, which is measured easier than the intensity ratio, as $\Delta C\ (cm^{-3}) \simeq 2.7\times10^{16}\Delta A_{PL}/A_{Raman(1200)}$, where ΔA_{PL} is the change in the peak PL amplitude and $A_{Raman(1200)}$ is the amplitude of the Raman band arbitrarily defined as the height of the spectrum point at 1200 cm^{-1} from the ordinate origin.

Electron transfer into the unoccupied molecular orbitals of O_2 induces optical absorption bands at much higher energies. Gaseous O_2 shows an intense absorption band

[1] In the TDS experiment reported in Ref. [20] we overestimated the amount of desorbed O_2 because we were unaware that the mass spectrometer indicated larger values than the actual partial pressures of O_2 at low pressure ranges where the desorption of O_2 was measured.

[2] The experimental procedure was identical to that described in Ref. [20]. The type of the sample used in this study was different from that used in Ref. [20] ('LowOH', SiOH $\sim 2\times10^{18}\,cm^{-3}$). However, these samples exhibit nearly the same PL quantum yield of interstitial O_2 as shown in Ref. [16]. Thus, the sample difference does not influence the result.

[3] The uneven uncertainty is due to the possible conversion of O_2 into H_2O, CO, and CO_2 through reactions with adsorbates on the sample and contaminants in the TDS chamber. In Ref. [20], this effect was also overlooked but was less serious than the overestimation of the amount of O_2 desorbed.

[4] We assumed that interstitial O_2 is equally lost from all the surfaces. On the other hand, the PL–Raman measurements probe only the two largest surfaces. Thus, the concentration change can be calculated by $\sim 8.3\times10^{16}/23\times2/0.1 \simeq 7.2\times10^{16}\,cm^{-3}$.

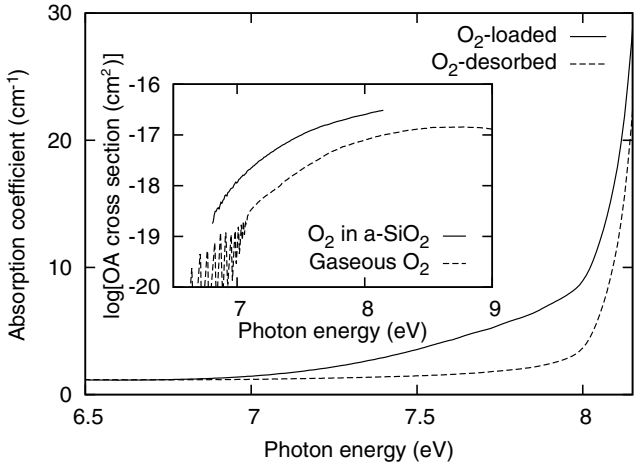

Fig. 4. VUV absorption spectra of a 1 mm-thick O_2-loaded (at 900 °C) a-SiO_2 sample before and after O_2 desorption in vacuum for 192 h at 900 °C (O_2 concentration change $\sim 2.1 \times 10^{17}$ cm^{-3}). The inset shows optical absorption (OA) cross section spectra of interstitial O_2 in a-SiO_2 and gaseous O_2. After Refs. [20,24]. The values of the OA cross section of interstitial O_2 have been revised following the TDS result presented in this paper.

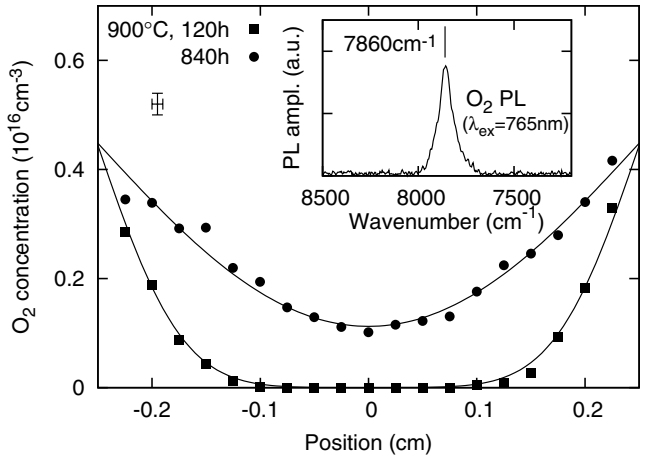

Fig. 5. Depth profile of O_2 concentration in a 0.5 cm-thick a-SiO_2 sample thermally annealed in air for 120 or 840 h at 900 °C, evaluated by measuring the intensity of the PL band at 1272 nm (shown in the inset, peak wavenumber at 7860 cm^{-1}) at each position at room temperature. Sample surfaces are at ±0.25 cm positions. The upper left bars indicate the relative errors. Solid lines are theoretical curves drawn by fitting to the data points. After Refs. [35,36]. The concentration values have been revised following the TDS result presented in this paper.

consisting of a vibrational structure (the Schumann–Runge (S–R) system, ~200–175 nm) and a continuous part (the S–R continuum, $\lesssim$200 nm), both attributed to the $B^3\Sigma_u^- \leftarrow X^3\Sigma_g^-$ transition [21,22]. The term 'vacuum-ultraviolet' (VUV) in fact stems from this absorption of O_2, which significantly blocks the propagation of wavelengths below ~200 nm unless air is evacuated. Interstitial O_2 in a-SiO_2 shows a VUV absorption band of the same origin [23]. However, its absorption spectrum is shifted to lower energy side and is more intense as shown in Fig. 4, probably because of the London dispersion interaction between interstitial O_2 and surrounding Si–O network [20,24].[5] Photoexcitation of the VUV absorption band of O_2 results in the cleavage of the O–O bond, as described in Section 3.1.

2.2. Thermal diffusion

Isotope labeling is a common technique to investigate the diffusion of mobile species. In a silicon substrate oxidized first by $^{16}O_2$ followed by $^{18}O_2$, two ^{18}O-rich SiO_2 layers are formed near the outer surface and the silicon–oxide interface [25–29]. This observation indicates that there are two types of mobile oxygen species whose properties are largely different. The ^{18}O-rich layer near the outer surface has been believed to be formed by the diffusion of the network oxygen; however, recent reports have indicated the importance of residual water in determining the ^{18}O profile [5,30]. In contrast, the oxygen flow that forms the interface ^{18}O-rich layer has been attributed to interstitial oxygen species, which migrate thorough interstitial voids without extensive interactions with the Si–O network [6,30–32]. This oxygen flow evidently governs the thermal oxidation of silicon. The solubility and diffusion coefficient of the interstitial oxygen species have been evaluated by measuring the amount of oxygen passing through thin a-SiO_2 plates (permeation method) [33]. This experiment have further confirmed that the solubility depends linearly on ambient O_2 pressure, strongly suggesting that the diffusing species is interstitial O_2.

The PL technique described in Section 2.1 is sensitive enough to study the dissolution and diffusion of O_2 in a-SiO_2 caused by thermal annealing in air [34–36]. Fig. 5 shows the depth distribution of interstitial O_2 in a-SiO_2 treated at 900 °C in air. The O_2 concentration is nearly constant at the sample surface irrespective of the annealing time, verifying that the surface dissolution of O_2 is much faster than the following diffusion of interstitial O_2 in a-SiO_2. The solubility[6] and diffusion coefficient of interstitial O_2 determined in this way agree well with those evaluated from the permeation experiment [33], the growth rate of SiO_2 films on silicon [1], and by a method utilizing the conversion of interstitial O_2 into SiOH groups reported recently (see also Section 2.3) [37]. Thus, it is confirmed that interstitial O_2 dominates the long range oxygen transport in a-SiO_2. The activation energy for the diffusion of

[5] The value of the concentration change of interstitial O_2, $\sim 4.7 \times 10^{16}$ cm^{-3}, described to explain Fig. 1 on page 2304 of Ref. [24] is incorrect. It should read $\sim 2.4 \times 10^{17}$ cm^{-3}. The correct value was used in the calculation and plots presented in Ref. [24]. However, all the concentration values of interstitial O_2 presented in Ref. [24], including the value shown above, should be decreased by ~12% on the bases of the TDS result presented in this paper. See also Fig. 4 in this paper.

[6] We revise the solubility preexponential factor S_0 reported in Ref. [36] as $4.2 \times 10^{15\pm0.2}$ cm^{-3} atm^{-1} (LowOH) and $4.8 \times 10^{15\pm0.2}$ cm^{-3} atm^{-1} (HighOH) (decrease of ~12%) on the bases of the TDS result presented in this paper.

interstitial O_2 is ~0.8–1.2 eV and is nearly constant between ~600–1200 °C [33,35–38].

Growth rate of a-SiO_2 films thinner than ~20–25 nm does not follow the linear-parabolic kinetics predicted by the Deal–Grove model [1]. Thermal oxidation rates at the corners of silicon step edges [39] and that of silicon nanoparticles [40] and nanorods [41] are smaller than the rate for flat wafers. These phenomena are most likely due to slow diffusion of interstitial O_2 in a stressed a-SiO_2 layer near the silicon–oxide interface, which is formed by the volume expansion that accompanies the oxidation [39,42,43]. Models that introduce such a modified a-SiO_2 layer with slow O_2 diffusion explain the actual growth kinetics well [44,45]. On the other hand, X-ray reflectivity observations have evidenced the presence of compressed a-SiO_2 layer with density ~2.4 g cm^{-3} (~2.2 g cm^{-3} for normal a-SiO_2) [46,47]. Theoretical calculations as well support the slow diffusion of interstitial O_2 in the compressed a-SiO_2 layer [48–50].

2.3. Reactions with hydrogen atoms, hydrogen molecules, and network-bound point defects

O_2 is reactive since it has unpaired spins (Fig. 1). H_2 cracks an Si–O bond as

$$\equiv Si{-}O{-}Si\equiv + H_2 \rightarrow \equiv SiOH + HSi\equiv \quad (1)$$

However, H_2 loading in a-SiO_2 containing interstitial O_2 causes a relatively rapid formation of SiOH groups with little accompanying creation of hydride (SiH) groups [51,52]. This observation has been interpreted by a two step process wherein interstitial O_2 first reacts with H_2 to form H_2O, and the resultant H_2O then hydrolyzes the Si–O network [53]:

$$1/2O_2 + H_2 \rightarrow H_2O \quad (2)$$

$$\equiv Si{-}O{-}Si\equiv + H_2O \rightarrow 2\equiv SiOH \quad (3)$$

The reaction of interstitial O_2 with H_2 (Eq. (2)) has been confirmed by a PL observation of the complete decomposition of interstitial O_2 after H_2 loading [54]. Recently, these reactions have been used to study the diffusion of interstitial O_2 [37]. O_2-rich a-SiO_2 samples (Suprasil W) are thermally annealed in vacuum to partially remove the dissolved interstitial O_2. Then the remaining interstitial O_2 is converted to SiOH group by H_2 loading because the concentration of SiOH groups is easily determined by the IR absorption spectroscopy [19,55–57]. The evaluated diffusion coefficients and those determined from the PL technique described in Section 2.2 [35,36] are in excellent agreement.

Hydrogen atom (H^0) is highly mobile in a-SiO_2 because of the small atomic size. It is metastable but is efficiently created by the F_2 laser photolysis of SiOH groups (quantum yield >0.1) [58–60]. Reaction of H^0 with interstitial O_2 produces interstitial hydroperoxy radical ($HO_2^{\cdot}$) [61]. This reaction is further described in Section 5.

Above ~400–500 °C interstitial O_2 becomes mobile and reacts with network-bound point defects. Reaction between interstitial O_2 and the silicon dangling bond (E' center, $\equiv Si^{\cdot}$)

$$\equiv Si^{\cdot} + O_2 \rightarrow \equiv SiOO^{\cdot} \quad (4)$$

is a major formation route of peroxy radical (POR, $\equiv SiOO^{\cdot}$) [62–64]. This reaction is slowed down by high-pressure densification of a-SiO_2 [65], consistent with the idea that interstitial O_2 is less mobile in compressed a-SiO_2 (Section 2.2). Interstitial O_2 oxidizes oxygen deficiency centers in a-SiO_2, such as Si–Si bond and divalent silicon, to eliminate optical absorption and PL bands associated with these centers [66,67]. It also oxidizes chloride (SiCl) groups to interstitial Cl_2 [54]:

$$2\equiv SiCl + 1/2O_2 \rightarrow \equiv Si{-}O{-}Si\equiv + Cl_2 \quad (5)$$

3. Interstitial oxygen atoms

3.1. Formation mechanisms

Cleavage of Si–O bond into a pair of dangling bonds

$$\equiv Si{-}O{-}Si\equiv \xrightarrow{h\nu} \equiv SiO^{\cdot} + {\cdot}Si\equiv \quad (6)$$

is an intrinsic radiation-induced defect process in a-SiO_2. However, this mechanism does not yield mobile oxygen species and thus cannot account for the formation of POR in high-purity O_2-free a-SiO_2 exposed to focused ArF laser light [63]. Dense electronic excitation forms self-trapped excitons (STE) in a-SiO_2. Optical studies of a-SiO_2 exposed to electron pulses [68] and α-quartz exposed to X-rays [69] have suggested that the formation of STE is accompanied by a large transient displacement of the bridging oxygen atom. Theoretical calculations have also predicted that a part of STEs relaxes into pairs of oxygen vacancies (Si–Si bond) and interstitial oxygen atoms (O^0) (Frenkel pair) [70,71]:

$$\equiv Si{-}O{-}Si\equiv \xrightarrow{h\nu} \equiv Si{-}Si\equiv + O^0 \quad (7)$$

A convincing result in favor of reaction Eq. (7) has been presented by proton implantation in a-SiO_2, where interstitial O_2 ('O^0 dimer') is found to be formed along with the Si–Si bonds as shown in Fig. 6 [72]. The following detections of interstitial O_2 in a-SiO_2 exposed to γ-rays [14] and electron beam [73] have confirmed that reaction Eq. (6) commonly occurs in a-SiO_2 subjected to the dense electronic excitation.

Another way to form interstitial O^0 is to photolyze interstitial O_2 (Section 2.1) using VUV light sources such as ArF ($\lambda = 193$ nm, $h\nu = 6.4$ eV) [23] and F_2 ($\lambda = 157$ nm, $h\nu = 7.9$ eV) lasers [74,75]

$$O_2 \xrightarrow{h\nu} 2O^0 \quad (8)$$

F_2 laser light, which is strongly absorbed by interstitial O_2, causes the photolysis Eq. (8) very efficiently.

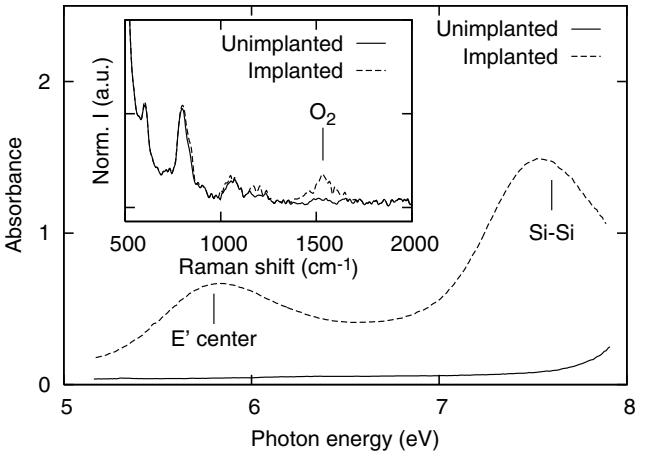

Fig. 6. Optical absorption and PL–Raman (inset) spectra of a proton-implanted a-SiO_2 sample, showing simultaneous formation of interstitial O_2 and Si–Si bonds by the Frenkel mechanism Eq. (7). After Ref. [72].

Decomposition of POR also yields O^0. POR has a weak optical absorption band at ~5 eV [76–78]. Photoexcitation into this absorption band decomposes POR [79], by dissociating the O–O bond to form a pair of the oxygen dangling bond (non-bridging oxygen hole center, NBOHC, $\equiv SiO^{\cdot}$) and O^0 [76,77,80]:

$$\equiv SiOO^{\cdot} \xrightarrow{h\nu} \equiv SiO^{\cdot} + O^0 \tag{9}$$

The photolysis quantum yield of POR by KrF laser light ($\lambda = 248$ nm, $h\nu = 5.0$ eV) is ~0.1 [80]. Other organic peroxy radicals and $HO_2^{\cdot}$ undergo similar UV photolysis reactions [81]. X-rays destroy PORs as well [82–84]; while earlier works [82,83] indicated that the bleaching of POR by X-rays is due to a separation of an O_2 molecule from the silicon atom, a more recent evidence [84] shows that the dominant process is most likely the same as the UV photolysis (Eq. (9)).

3.2. Configuration in a-SiO_2 network

Theoretical studies have indicated that interstitial O^0 forms an Si–O–O–Si bond (peroxy linkage, POL; peroxy bridge) rather than is isolated in the interstitial voids [85–88], and that O^0 of the POL configuration exhibits a weak VUV absorption band [89,90]. The predicted peak parameters are close to that of a weak absorption band induced at ~7.1 eV by F_2 laser photolysis of interstitial O_2 (Eq. (8)) [74]. Furthermore, a recent X-ray diffraction study has shown that the migration of interstitial O^0 is accompanied by a significant rearrangement of the Si–O network, which is not caused by the diffusion of interstitial O_2 [91]. Thus, interstitial O^0 probably forms POL in the Si–O network.

3.3. Thermal diffusion and reactions

Oxidation of silicon by O^0 below ~500–600 °C is a promising technique to fabricate thin gate dielectric oxide films while avoiding undesirable phenomena occurring at high temperatures [92–97]. Mobility of O^0 in a-SiO_2 can be studied via the rate of the dimerization of O^0s (reverse reaction of Eq. (8)), which is measured by monitoring the formation of interstitial O_2 using the PL technique (Section 2.1). Fig. 7 shows the concentration change of interstitial O_2 with F_2 laser photolysis at 77 K followed by sequential thermal annealing steps at several temperatures [75]. O^0 becomes mobile above ~200 °C and is mostly converted back to interstitial O_2 after heating above 400 °C. This temperature range coincides with that of the silicon oxidation by O^0 [93,95,97].

The activation energy for the diffusion of O^0 in a-SiO_2 remains controversial. The activation energy evaluated from the dimerization rate (~1.0–1.5 eV [74,75]) is in accord with a theoretical calculation predicting the diffusion of O^0 as POL [86]. However, the activation energy of the parabolic rate constant of the O^0 oxidation is much small (~0.1–0.4 eV) [94–97].

Mobile O^0 transforms NBOHC to POR [77,80,98]:

$$\equiv SiO^{\cdot} + O^0 \rightarrow \equiv SiOO^{\cdot} \tag{10}$$

Thus, NBOHC and POR convert to each other via reactions Eqs. (9) and (10). Observations suggest that reaction of O^0 with E' center

$$\equiv Si^{\cdot} + O^0 \rightarrow \equiv SiO^{\cdot} \tag{11}$$

also takes place [12,80]. The reaction Eq. (10) is slower in a sample with a higher fictive temperature [99], implying that O^0 is less mobile in more disordered a-SiO_2 network.

F_2 laser irradiation to a-SiO_2 containing both SiCl groups and interstitial O_2 produces interstitial chlorine-related radicals ($ClO_x^{\cdot}$ where $x = 2, 3$) [100]. However, F_2 laser light alone does not dissociate the Si–Cl bond [54]. Thus, the most probable mechanism of the formation of

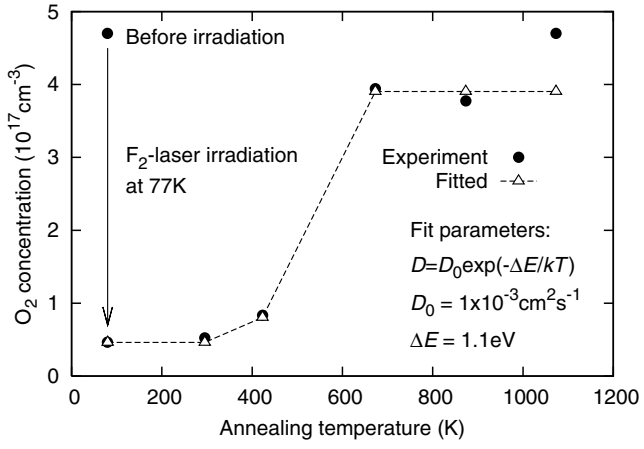

Fig. 7. Concentration change of interstitial O_2 by F_2 laser irradiation at 77 K followed by sequential thermal annealings steps at 150, 400, 600, and 800 °C (15 min at each step). Open triangles and dotted lines are calculated by fitting to the experimental data points (solid circles). The activation energy for diffusion of O^0 (ΔE) and the preexponential factor (D_0) obtained from the fit are shown. After Ref. [75].

$ClO_x^{\cdot}$ is the cracking of SiCl groups by O^0 generated via the F_2 laser photolysis of interstitial O_2, and following oxygen addition to the reaction intermediates.

4. Interstitial ozone molecules

Interstitial ozone molecules (O_3) are formed via reaction of interstitial O_2 with O^0 photogenerated by exposure to ArF [23] or F_2 [101] laser light

$$3/2O_2 \xrightarrow{h\nu} O_3 \tag{12}$$

An analogous reaction that involves the thermal diffusion of O^0 is unlikely to occur because O_3 decomposes above ~200 °C. Interstitial O_3 has an optical absorption band at ~4.8 eV. Unfortunately, this band almost overlaps with the 4.8 eV absorption band of NBOHC, one of the most frequently observed color centers in a-SiO_2. This overlap is the most probable reason for poor intensity correlation between optical absorption at 4.8 eV and the 1.9 eV PL band of NBOHC in F_2-laser-irradiated O_2-rich a-SiO_2 [102].

Interstitial O_3 is decomposed by UV light ($h\nu \gtrsim 4$ eV) without changing the NBOHC concentration, making it possible to extract the peak parameters of the absorption band of interstitial O_3 [101]. The UV photolysis yields excited interstitial O_2 ($a^1\Delta_g$) (Fig. 1) and O^0 (^1D). The excited interstitial O_2 generated in this way as well induces the characteristic IR PL band of singlet O_2 (Section 2.1, Fig. 1), which is useful in verifying the presence of interstitial O_3 [101].

5. Interstitial reactive oxygen radicals

Reactive oxygen radicals such as $O^{\cdot -}$, $O_2^{\cdot -}$ (superoxide ion radical), and $O_3^{\cdot -}$ (ozonide ion radical) are important oxidants in the catalytic oxidation reactions. Their conjugated bases, $HO^{\cdot}$ (hydroxyl radical), $HO_2^{\cdot}$ (hydroperoxy radical), and $HO_3^{\cdot}$ (hydrogen trioxide radical) are also involved in reactions in acidic solutions and protic solvents. Since a-SiO_2 is an important catalytic support and even a heterogeneous catalyst, it is of interest to study interactions of a-SiO_2 with reactive oxygen radicals.

Fig. 8 shows electron paramagnetic resonance (EPR) spectra of interstitial $HO_2^{\cdot}$ and $HO^{\cdot}$ in a-SiO_2. Interstitial $HO_2^{\cdot}$ is formed by reactions of interstitial O_2 with H^0 [61]

$$O_2 + H^0 \rightarrow HO_2^{\cdot} \tag{13}$$

The same reaction occurs in the gas phase but the reaction requires a third body M, which takes away the heat of the reaction, to generate $HO_2^{\cdot}$ efficiently [103–105]

$$O_2 + H^0 + M \rightarrow HO_2^{\cdot} + M \tag{14}$$

Thus, in a-SiO_2 the Si–O network serves the role of M that dissipates the excess energy of the reaction intermediate. Although $HO_2^{\cdot}$ is highly reactive, the trapping in chemically inert a-SiO_2 interstices makes $HO_2^{\cdot}$ thermally stable up to ~100 °C.

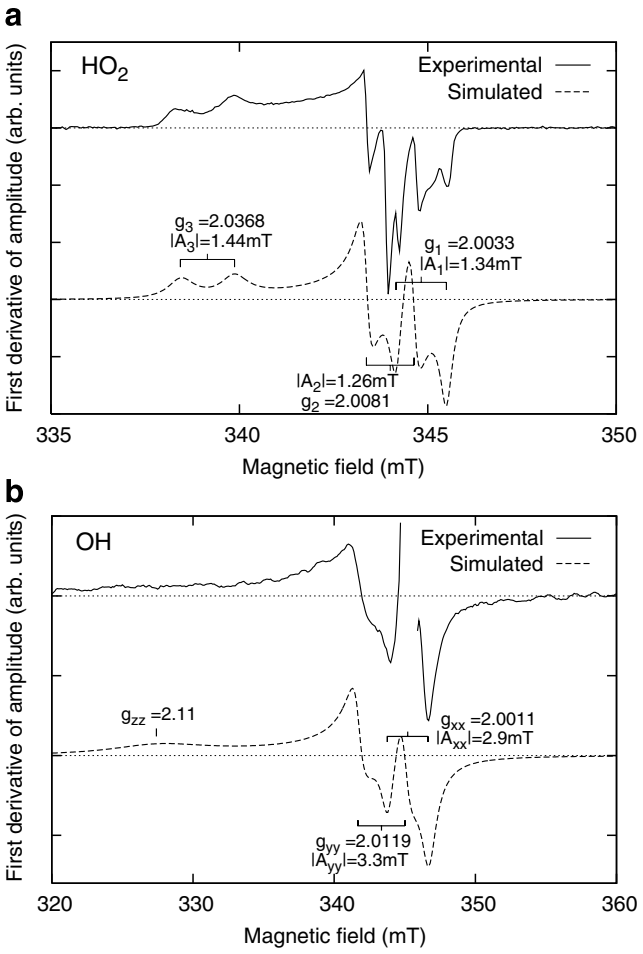

Fig. 8. Experimental and simulated EPR spectra of HO_2 and OH radicals in a-SiO_2 (measured at 77 K; microwave power, 20 mW; modulation amplitude, 0.1 mT for HO_2 radical and 0.2 mT for OH radical). After Refs. [61,106].

Interstitial $HO^{\cdot}$ is formed by photolyzing interstitial H_2O with F_2 laser light at 77 K [106]

$$H_2O \xrightarrow{h\nu} HO^{\cdot} + H^0 \tag{15}$$

EPR spectra of $HO^{\cdot}$ in a-SiO_2 (Fig. 8) and in amorphous ice [107] are similar to each other, indicating that the detected $HO^{\cdot}$ is confined by hydrogen bonding with adjacent H_2O molecules and SiOH groups. The hydrogen bonding quenches the angular momentum of the doubly-degenerate O 2pπ orbitals accommodating the unpaired spin, and allows interstitial $HO^{\cdot}$ to be detectable by EPR. The decomposition of $HO^{\cdot}$ occurs above ~150 K simultaneously with the formation of $HO_2^{\cdot}$. The creation of $HO_2^{\cdot}$ is not due to reaction Eq. (13), but rather due to the reaction of $HO^{\cdot}$ with O^0

$$HO^{\cdot} + O^0 \rightarrow HO_2^{\cdot} \tag{16}$$

because the sample is initially O_2 free but O^0 is formed by F_2 laser photolysis of $HO^{\cdot}$.

$HO_3^{\cdot}$, which has been generated in solid Ar matrices [108], has not been found in a-SiO_2 yet. Charged radicals such as $O^{\cdot -}$, $O_2^{\cdot -}$, and $O_3^{\cdot -}$ can be formed on surfaces of porous a-SiO_2 [109] but are unlikely to be trapped in neutral a-SiO_2 network. Paramagnetic species found in some non-porous a-SiO_2 samples exposed to γ-rays [109,110] may be $HO_2^{\cdot}$ rather than $O_2^{\cdot -}$. Recently, a new EPR signal, probably attributed to oxygen related centers, has been reported in heavily O^+-ion-implanted a-SiO_2, in which a large fraction of the implanted oxygen is considered to be turned to interstitial species [111].

6. Summary

Oxygen molecules (O_2) incorporated in the interstitial voids in a-SiO_2 play a central role in diffusion and reactions of oxygen species in a-SiO_2, and the characteristic infrared (IR) photoluminescence (PL) of interstitial O_2 is very useful in studying these processes. The IR PL band at $\lambda = 1272$ nm due to the $a^1\Delta_g \rightarrow X^3\Sigma_g^-$ transition of O_2 is induced by excitation with a continuous-wave titanium sapphire laser operated at $\lambda = 765$ nm or a Nd-doped solid-state laser oscillating at $\lambda = 1064$ nm. The quantitative relation between the PL intensity measured at room temperature and the concentration of interstitial O_2 is calibrated by the thermal desorption spectroscopy. Results obtained by the PL method confirm that the mobile species dominating the thermal oxygen transport in a-SiO_2 is interstitial O_2. The dissolution of O_2 from ambient atmosphere is much faster than the following diffusion of O_2 in a-SiO_2. Exposure to F_2 laser light ($\lambda = 157$ nm, $h\nu = 7.9$ eV) efficiently decomposes interstitial O_2 by dissociating the O–O bond. The resultant interstitial atoms (O^0) are most likely embedded in the Si–O network by forming Si–O–O–Si bonds. Interstitial O^0 becomes mobile above ~200 °C. The mobility of O^0 in a-SiO_2 is evaluated from the rate of recovery of O_2 by thermal annealing. Other reactions involving O^0 include the radiation-induced decomposition of an Si–O–Si bond into a pair of Si–Si bond and O^0 (Frenkel process), conversion between the oxygen dangling bond (≡$SiO^{\cdot}$) and peroxy radical (≡$SiOO^{\cdot}$), and formation of interstitial ozone molecules (O_3). Interstitial hydroxyl ($HO^{\cdot}$) and hydroperoxy ($HO_2^{\cdot}$) radicals are created by photochemical reactions involving interstitial hydrogen and oxygen species in a-SiO_2.

References

[1] B.E. Deal, A.S. Grove, J. Appl. Phys. 36 (1965) 3770.
[2] G. Pacchioni, L. Skuja, D.L. Griscom (Eds.), Defects in SiO_2 and Related Dielectrics: Science and Technology, NATO Science Series, Kluwer Academic, Dordrecht, Netherlands, 2000.
[3] R.A.B. Devine, J.P. Duraud, E. Dooryhée (Eds.), Structure and Imperfections in Amorphous and Crystalline Silicon Dioxide, John Wiley, Chichester, England, 2000.
[4] J.E. Shelby, Handbook of Gas Diffusion in Solids and Melts, ASM International, Materials Park, 1996.
[5] R.H. Doremus, Diffusion of Reactive Molecules in Solids and Melts, John Wiley, New York, 2002.
[6] M.A. Lamkin, F.L. Riley, R.J. Fordham, J. Euro. Ceram. Soc. 10 (1992) 347.
[7] W. Carvalho, P. Dumas, J. Corset, V. Newman, J. Raman Spectrosc. 16 (1985) 330.
[8] K. Nassau, J.W. Shiever, Am. Ceram. Soc. Bull. 54 (1975) 1004.
[9] C. Schweitzer, R. Schmidt, Chem. Rev. 103 (2003) 1685.
[10] W. Heitmann, H.U. Bonewitz, A. Mühlich, Electron. Lett. 19 (1983) 616.
[11] L. Skuja, in: G. Pacchioni, L. Skuja, D.L. Griscom (Eds.), Defects in SiO_2 and Related Dielectrics: Science and Technology, NATO Science Series, Kluwer Academic, Dordrecht, Netherlands, 2000, p. 73 (See Ref. [2]).
[12] L. Skuja, B. Güttler, Phys. Rev. Lett. 77 (1996) 2093.
[13] T. Shikama, M. Narui, T. Kakuta, H. Kayano, T. Sagawa, K. Sanada, Nucl. Instrum. Methods Phys. Res. B 91 (1994) 342.
[14] L. Skuja, B. Güttler, D. Schiel, A.R. Silin, Phys. Rev. B 58 (1998) 14296.
[15] L. Skuja, B. Güttler, D. Schiel, Glass Sci. Technol. – Glastech. Ber. 71C (1998) 73.
[16] K. Kajihara, H. Kamioka, M. Hirano, T. Miura, L. Skuja, H. Hosono, J. Appl. Phys. 98 (2005) 013528.
[17] R.M. Badger, A.C. Wright, R.F. Whitlock, J. Chem. Phys. 43 (1965) 4345.
[18] L. Skuja, B. Güttler, D. Schiel, A.R. Silin, J. Appl. Phys. 83 (1998) 6106.
[19] Y. Morimoto, T. Igarashi, H. Sugahara, S. Nasu, J. Non-Cryst. Solids 139 (1992) 35.
[20] K. Kajihara, M. Hirano, M. Uramoto, Y. Morimoto, L. Skuja, H. Hosono, J. Appl. Phys. 98 (2005) 013527.
[21] K. Watanabe, E.C.Y. Inn, M. Zelikoff, J. Chem. Phys. 21 (1953) 1026.
[22] K. Watanabe, Adv. Geophys. 5 (1958) 153.
[23] K. Awazu, H. Kawazoe, J. Appl. Phys. 68 (1990) 3584.
[24] K. Kajihara, M. Hirano, L. Skuja, H. Hosono, J. Non-Cryst. Solids 352 (2006) 2303.
[25] R. Rosencher, A. Straboni, S. Rigo, G. Amsel, Appl. Phys. Lett. 34 (1979) 254.
[26] F. Rochet, B. Agius, S. Rigo, J. Electrochem. Soc. 131 (1984) 914.
[27] J.A. Costello, R.E. Tressler, J. Electrochem. Soc. 131 (1984) 1944.
[28] C.J. Han, C.R. Helms, J. Appl. Phys. 59 (1986) 1767.
[29] C.-J. Han, C.R. Helms, J. Electrochem. Soc. 135 (1988) 1824.
[30] R.H. Doremus, J. Non-Cryst. Solids 349 (2004) 242.
[31] A. Bongiorno, A. Pasquarello, Phys. Rev. Lett. 88 (2002) 125901.
[32] W. Orellana, A.J.R. da Silva, A. Fazzio, Phys. Rev. Lett. 87 (2001) 155901.
[33] F.J. Norton, Nature 191 (1961) 701.
[34] K. Kajihara, T. Miura, H. Kamioka, M. Hirano, L. Skuja, H. Hosono, J. Non-Cryst. Solids 349 (2004) 205.
[35] K. Kajihara, T. Miura, H. Kamioka, M. Hirano, L. Skuja, H. Hosono, J. Ceram. Soc. Jpn. 112 (2004) 559.
[36] K. Kajihara, H. Kamioka, M. Hirano, T. Miura, L. Skuja, H. Hosono, J. Appl. Phys. 98 (2005) 013529.
[37] C.C. Tournour, J.E. Shelby, Phys. Chem. Glasses 46 (2005) 559.
[38] K. Kajihara, unpublished.
[39] R.B. Marcus, T.T. Sheng, J. Electrochem. Soc. 129 (1982) 1278.
[40] R. Okada, S. Iijima, Appl. Phys. Lett. 58 (1991) 1662.
[41] H.I. Liu, D.K. Biegelsen, F.A. Ponce, N.M. Johnson, R.F.W. Pease, Appl. Phys. Lett. 64 (1994) 1383.
[42] A. Fargeix, G. Ghibaudo, G. Kamarinos, J. Appl. Phys. 54 (1983) 2878.
[43] R.H. Doremus, J. Appl. Phys. 66 (1989) 4441.
[44] N.F. Mott, S. Rigo, F. Rochet, A.M. Stoneham, Philos. Mag. B 60 (1989) 189.
[45] T. Watanabe, K. Tatsumura, I. Ohdomari, Phys. Rev. Lett. 96 (2006) 196102.

[46] N. Awaji, S. Ohkubo, T. Nakanishi, Y. Sugita, K. Takasaki, S. Komiya, Jpn. J. Appl. Phys. 35 (1996) L67.
[47] S.D. Kosowsky, P.S. Pershan, K.S. Krisch, J. Bevk, M.L. Green, D. Brasen, L.C. Feldmana, P.K. Roy, Appl. Phys. Lett. 70 (1997) 3119.
[48] A. Bongiorno, A. Pasquarello, Phys. Rev. B 70 (2004) 195312.
[49] T. Akiyama, K. Kawamoto, H. Kageshima, M. Uematsu, K. Nakamura, T. Ito, Thin Solid Films 508 (2006) 311.
[50] L. Tsetseris, S.T. Pantelides, Phys. Rev. Lett. 97 (2006) 116101.
[51] J.E. Shelby, J. Appl. Phys. 51 (1980) 2589.
[52] J.M. Wiesenfeld, J. Stone, D. Marcuse, C.A. Burrus, S. Yang, J. Appl. Phys. 61 (1987) 5447.
[53] J.E. Shelby, J. Non-Cryst. Solids 179 (1994) 138.
[54] K. Kajihara, M. Hirano, L. Skuja, H. Hosono, J. Appl. Phys. 98 (2005) 043515.
[55] J.E. Shelby, J. Vitko Jr., R.E. Benner, J. Am. Ceram. Soc. 65 (1982) C59.
[56] K.M. Davis, M. Tomozawa, J. Non-Cryst. Solids 201 (1996) 177.
[57] K.M. Davis, A. Agarwal, M. Tomozawa, K. Hirao, J. Non-Cryst. Solids 203 (1996) 27.
[58] K. Kajihara, L. Skuja, M. Hirano, H. Hosono, Appl. Phys. Lett. 79 (2001) 1757.
[59] K. Kajihara, L. Skuja, M. Hirano, H. Hosono, Phys. Rev. Lett. 89 (2002) 135507.
[60] K. Kajihara, L. Skuja, M. Hirano, H. Hosono, Phys. Rev. B 74 (2006) 094202.
[61] K. Kajihara, M. Hirano, L. Skuja, H. Hosono, J. Am. Chem. Soc. 128 (2006) 5371.
[62] A.H. Edwards, W.B. Fowler, Phys. Rev. B 26 (1982) 6649.
[63] T.E. Tsai, D.L. Griscom, Phys. Rev. Lett. 67 (1991) 2517.
[64] R.L. Pfeffer, in: R.A.B. Devine (Ed.), The Physics and Technology of Amorphous SiO_2, Plenum, New York, 1988, p. 181.
[65] R.A.B. Devine, J.J. Capponi, J. Arndt, Phys. Rev. B 35 (1987) 770.
[66] G. Hetherington, K.H. Jack, Phys. Chem. Glasses 5 (1964) 147.
[67] H. Imagawa, T. Arai, H. Hosono, H. Imai, K. Arai, J. Non-Cryst. Solids 179 (1994) 70.
[68] K. Tanimura, T. Tanaka, N. Itoh, Phys. Rev. Lett. 51 (1983) 423.
[69] H. Hayes, M.J. Kane, O. Salminen, R.L. Wood, S.P. Doherty, J. Phys. C 17 (1984) 2943.
[70] A. Shluger, E. Stefanovich, Phys. Rev. B 42 (1990) 9664.
[71] A.L. Shluger, J.L. Gavartin, M.A. Szymanski, A.M. Stoneham, Nucl. Instrum. Methods Phys. Res. B 166&167 (2000) 1.
[72] H. Hosono, H. Kawazoe, N. Matsunami, Phys. Rev. Lett. 80 (1998) 317.
[73] M.A. Stevens-Kalceff, Phys. Rev. Lett. 84 (2000) 3137.
[74] L. Skuja, K. Kajihara, T. Kinoshita, M. Hirano, H. Hosono, Nucl. Instrum. Methods Phys. Res. B 191 (2002) 127.
[75] L. Skuja, M. Hirano, K. Kajihara, H. Hosono, Phys. Chem. Glasses 43C (2002) 145.
[76] V.A. Radzig, in: G. Pacchioni, L. Skuja, D.L. Griscom (Eds.), Defects in SiO_2 and Related Dielectrics: Science and Technology, NATO Science Series, Kluwer Academic, Dordrecht, Netherlands, 2000, p. 339, See Ref. [2].
[77] L. Skuja, M. Hirano, H. Hosono, K. Kajihara, A. Silin, Glass Sci. Technol. – Glastech. Ber. 75 (2002) 24.
[78] C. Sousa, C. de Graaf, G. Pacchioni, J. Chem. Phys. 114 (2001) 6259.
[79] H. Hosono, R.A. Weeks, J. Non-Cryst. Solids 116 (1990) 289.
[80] K. Kajihara, L. Skuja, M. Hirano, H. Hosono, Phys. Rev. Lett. 92 (2004) 015504.
[81] P.D. Lightfoot, R.A. Cox, J.N. Crowley, M. Destriau, G.D. Hayman, M.E. Jenkin, G.K. Moortgat, F. Zabel, Atmos. Environ. A 26 (1992) 1805.
[82] L. Zhang, V.A. Mashkov, R.G. Leisure, Phys. Rev. Lett. 74 (1995) 1605.
[83] L. Zhang, V.A. Mashkov, R.G. Leisure, Phys. Rev. B 53 (1996) 7182.
[84] K. Kajihara, L. Skuja, M. Hirano, H. Hosono, Phys. Status Solidi C 2 (2005) 314.
[85] G. Pacchioni, G. Ieranó, Phys. Rev. B 56 (1997) 7304.
[86] D.R. Hamann, Phys. Rev. Lett. 81 (1998) 3447.
[87] K.-O. Ng, D. Vanderbilt, Phys. Rev. B 59 (1999) 10132.
[88] M.A. Szymanski, A.L. Shluger, A.M. Stoneham, Phys. Rev. B 63 (2001) 224207.
[89] G. Pacchioni, G. Ieranó, Phys. Rev. B 57 (1998) 818.
[90] B.B. Stefanov, K. Raghavachari, J. Chem. Phys. 111 (1999) 8039.
[91] K. Tatsumura, T. Shimura, E. Mishima, K. Kawamura, D. Yamasaki, H. Yamamoto, T. Watanabe, M. Umeno, I. Ohdomari, Phys. Rev. B 72 (2005) 045205.
[92] K. Miyake, S. Kimura, T. Warabisako, H. Sunami, T. Tokuyama, J. Vac. Sci. Technol. A 2 (1984) 496.
[93] V. Nayar, P. Patel, I.W. Boyd, Electron. Lett. 26 (1990) 205.
[94] A. Kazor, I.W. Boyd, Electron. Lett. 23 (1991) 909.
[95] Y. Ishikawa, T. Shibamoto, I. Nakamichi, Jpn. J. Appl. Phys. 31 (1992) 1148.
[96] T. Ueno, A. Morioka, S. Chikamura, Y. Iwasaki, Jpn. J. Appl. Phys. 39 (2000) L327.
[97] T. Nishiguchi, H. Nonaka, S. Ichimura, Y. Morikawa, M. Kekura, M. Miyamoto, Appl. Phys. Lett. 81 (2002) 2190.
[98] D.L. Griscom, M. Mizuguchi, J. Non-Cryst. Solids 239 (1998) 66.
[99] K. Kajihara, L. Skuja, M. Hirano, H. Hosono, J. Non-Cryst. Solids 345&346 (2004) 219.
[100] H. Nishikawa, R. Nakamura, Y. Ohki, K. Nagasawa, Y. Hama, Phys. Rev. B 46 (1992) 8073.
[101] L. Skuja, M. Hirano, H. Hosono, Phys. Rev. Lett. 84 (2000) 302.
[102] J.H. Stathis, M.A. Kastner, Philos. Mag. B 49 (1984) 357.
[103] M.J. Kurylo, J. Phys. Chem. 76 (1972) 3518.
[104] L.C. Lee, J. Chem. Phys. 76 (1982) 4909.
[105] J.J. Schwab, W.H. Brune, J.G. Anderson, J. Phys. Chem. 93 (1989) 1030.
[106] K. Kajihara, M. Hirano, L. Skuja, H. Hosono, J. Phys. Chem. B 110 (2006) 10224.
[107] J. Bednarek, A. Plonka, A. Hallbrucker, E. Mayer, M.C.R. Symons, J. Am. Chem. Soc. 118 (1996) 9387.
[108] B. Nelander, A. Engdahl, T. Svensson, Chem. Phys. Lett. 332 (2000) 403.
[109] G. Kordas, R.A. Weeks, L.C. Klein, J. Non-Cryst. Solids 71 (1985) 327.
[110] H. Nishikawa, R. Tohmon, Y. Ohki, K. Nagasawa, Y. Hama, J. Appl. Phys. 65 (1989) 4672.
[111] R.H. Magruder III, A. Stesmans, K. Clemer, R.A. Weeks, R.A. Weller, J. Non-Cryst. Solids 352 (2006) 3027.